Digestive and Liver Disease 51 (2019) 397–411

Contents lists available at ScienceDirect

Digestive and Liver Disease

journal homepage: www.elsevier.com/locate/dld

Liver, Pancreas and Biliary Tract

MicroRNA-494-dependent WDHDI inhibition suppresses epithelial-mesenchymal transition, tumor growth and metastasis in cholangiocarcinoma

Bo Liu[a], Yu Hu[b], Lu Qin[c], Xu-Bin Peng[d], Ya-Xun Huang[a,*]

[a] Department of General Surgery, The Second Xiangya Hospital, Central South University, Changsha, PR China
[b] Center for Experimental Medical Research, Third Xiangya Hospital, Central South University, Changsha, PR China
[c] Department of Intestinal Surgery, The Affiliated Cancer Hospital of Xiangya School of Medicine, Central South University, Changsha, PR China
[d] Department of Neurosurgery, The Cancer Hospital Affiliated to Xiangya School of Medicine, Central South University, Changsha, PR China

ARTICLE INFO

Article history:
Received 31 March 2018
Received in revised form 16 August 2018
Accepted 21 August 2018
Available online 30 August 2018

Keywords:
MicroRNA-494
WDHD1
Cholangiocarcinoma
Epithelial-mesenchymal transition
Lymph node metastasis

ABSTRACT

Background: Cholangiocarcinoma (CCA) represents a devastating malignancy characterized by high mortality, and notoriously problematic to diagnose. Recently, microRNAs (miRs) have been intensively investigated due to their potential usefulness from a tumor treatment perspective.
Aims: The current study was aimed to investigate whether miR-494 influences epithelial-mesenchymal transition (EMT), tumor growth and metastasis of CCA.
Methods: The regulatory miRNAs of WDHD1 in CCA expression chip were predicted, followed by determination of the miR-494 and WDHD1 expression in normal cholangiocyte tissues and CCA tissues. The related protein levels were determined. CCA cell migration, invasion, viability, and cell cycle distribution and the dosage-dependent effect of miR-494 on CCA cell growth were subsequently detected. Finally, tumorigenicity and lymph node metastasis (LNM) were measured.
Results: Initially, miR-194 affected the CCA development via negatively regulating WDHD1 and miR-494 which were downregulated while WDHD1 was upregulated in CCA. In addition, miR-494 overexpression elevated E-cadherin expression while decreased expressions of WDHD1, N-cadherin, Vimentin, Snail, Twist and MMP-9. Finally, overexpressed miR-494 was observed to suppress EMT, cell viability, migration, invasion, arrest cell cycle progression, tumor formation, and LNM while accelerating cell apoptosis in vivo.
Conclusion: This study indicated that miR-494 overexpression suppresses EMT, tumor formation and LNM while promoting CCA cell apoptosis through inhibiting WDHD1 in CCA.
© 2018 Editrice Gastroenterologica Italiana S.r.l. Published by Elsevier Ltd. All rights reserved.

1. Introduction

Cholangiocarcinoma (CCA) also commonly referred to as bile duct cancer, represents a malignancy arising from cholangiocytes at varying locations within the lining of the biliary tree that exhibits numerous differentiation markers [1]. As a relatively rare but highly malignant invasive carcinoma, CCA is considered to be an intractable tumor with rapidly increasing incidence, mortality rates, and poor prognosis worldwide, particularly in East Asia [2]. A number of established CCA risk factors have been highlighted in various literatures including parasitic infections, primary sclerosing cholangitis, biliary-duct cysts, toxins and hepatolithiasis [3]. CCA is further sub-divided into intrahepatic cholangiocarcinoma (ICCA) and extrahepatic cholangiocarcinoma (ECCA) owing to its distinct etiological and clinical features; the latter is further subdivided into perihilar cholangiocarcinoma (pCCA or Klatskin tumor) and distal cholangiocarcinoma (dCCA), with a frequency between 10%–20% iCCA, 50% pCCA and 30%–40% eCCA [4,5]. A significant stumbling block remains the treatment of CCA due to its nature and typically clinically silent manifestation, leading to diagnosis during the later stages of the disease, with complete surgical resection remaining the most effective treatment option [6]. For many years, surgical resection has been the only curative treatment option for patients with CCA, with no feasible chemotherapy regimens available for the postoperative recurrence of CCA [7]. Therefore,

* Corresponding author at: Department of General Surgery, The Second Xiangya Hospital, Central South University, No. 139, Renmin Middle Road, Changsha 410011, Hunan, PR China.
E-mail address: hyxhuangyaxun@126.com (Y.-X. Huang).

https://doi.org/10.1016/j.dld.2018.08.021
1590-8658/© 2018 Editrice Gastroenterologica Italiana S.r.l. Published by Elsevier Ltd. All rights reserved.

a improved understanding of the molecular mechanisms related to CCA development is of high clinical significance.

Recently, CCA molecular profiling has revealed its potential from a targeted treatment therapy perspective [7]. MicroRNAs (miRs/miRNAs) represent endogenous non-coding RNAs that play crucial roles in a large array of biological processes, such as cell apoptosis, development and aging, the aberrant expression of which results in phenotypic features of malignant cells [8]. A previous study identified that miRNAs are dysregulated in CCA, aberrant dysregulations of which are pivotal in the genesis and progression of CCA. [9]. Low levels of miR-494 expression have recently emerged as a key mediator of CCA growth [10]. Another data source highlighted potential of WD repeat and high mobility group [HMG]-box DNA-binding protein 1 (WDHD1) as a candidate biomarker and a promising therapeutic target for cancer due to its important role in lung and esophageal carcinogenesis as a cell cycle regulator [11]. As a replisome component tasked with regulating DNA replication, WDHD1 induces DNA replication and modulates the G1 checkpoint, while the inhibition of WDHD1 results in a decline in the replication of human papillomavirus E7-expressing cells [12]. Moreover, reports have highlighted lymph node metastasis (LNM) and CCA to be indications of poor prognosis [13]. Epithelial-mesenchymal transition (EMT) has been reported to be a critical component for cancer progression, due to its ability to convert adherent epithelial cells into individual migratory cells, invading the extracellular matrix [14]. During the present study, we initially assessed the effects of miR-494 on EMT and LNM in CCA cells, in an attempt to elucidate the regulatory mechanism of miR-494 targeting WDHD1 on CCA development and progression, with the intention of presenting a theoretical foundation for an enhanced understanding of CCA treatment.

2. Materials and methods

2.1. Ethics statement

The current study was conducted with the approval of the ethics committee of the Second Xiangya Hospital, Central South University. All animal experiments were conducted in strict accordance with the Guide for the Care and Use of Laboratory Animals.

2.2. Microarray analysis

CCA expression chip GSE45001 was retrieved and downloaded from the Gene Expression Omnibus database (GEO, https://www.ncbi.nlm.nih.gov/geo/). The GSE45001 chip was comprised of 10 CCA samples and 10 normal control samples. The limma package in the R Programming Language was employed for the differential analysis of the CCA and normal samples on the chip with reference to p value <0.05 and |logFC| >2 as the screening threshold set in order to identify and obtain differentially expressed genes. Next, the UALCAN database (http://ualcan.path.uab.edu/cgi-bin/ualcan-res.pl) was used to retrieve WDHD1 expression in the Cancer Genome Atlas (TCGA) of CCA data. The MalaCards database (http://www.malacards.org/) was then explored to retrieve relevant CCA genes. The STRING database (https://string-db.org/) was utilized to construct an interaction network between the differentially expressed genes with the known genes of CCA, while the core analysis was preceded on the obtained interaction network using a cytoscape software.

On completion of the aforementioned, TargetScan database (http://www.targetscan.org/vert_71/), microRNA.org database (http://34.236.212.39/microrna/home.do), miRNAMap database (http://mirnamap.mbc.nctu.edu.tw/), mirDIP database (http://ophid.utoronto.ca/mirDIP/index.jsp#r) miRDB database (http://mirdb.org/miRDB/index.html) and TarBase database (http://carolina.imis.athena-innovation.gr/diana_tools/web/index.php?r=tarbasev8%2Findex&miRNAs%5B%5D=&genes%5B%5D=&publication_year=&prediction_score=&sort_field=&sort_type=&query=1) were used to predict the regulatory miRNAs of WDHD1 and the intersection of the predicted results from 6 databases was obtained.

2.3. Study subject

Between January 2012 and January 2017, CCA tissue samples were collected by means of surgical resection or biopsy from 135 patients pathologically confirmed with CCA in the Second Xiangya Hospital, Central South University. Amongst the 135 patients, 91 were male and 44 were female (mean age 60.42 ± 11.0 years), among which 41 patients were diagnosed with lymph nodes metastasis, 94 patients without lymph nodes metastasis, 35 patients with distant metastasis and 100 patients without distant metastasis. According to the Union for International Cancer Control and American Joint Committee on Cancer (UICC/AJCC) on CCA tumor-nodes-metastasis (TNM) classification, 96 patients were in I–II stage and 39 patients were in III–IV stage. In addition, normal cholangiocyte tissues from 34 CCA patients who underwent liver transplantation were regarded as the control group.

2.4. Cell culture and transfection

The human normal cholangiocyte cell line HIBEC and CCA cell lines QBC939 and RBE purchased from the American Type Culture Collection (ATCC) company (Manassas, VA, USA) were routinely cultured in a 5% CO_2 incubator at 37 °C. The cell lines were cultured in complete Roswell Park Memorial Institute (RPMI) 1640 medium containing 10% fetal bovine serum (FBS), 100 μ/mL penicillin and 100 mg/mL streptomycin. The cultured adhered cells were treated with 0.25% trypsin. Cells at the logarithmic growth phase were preserved for further experimentation while the expression of miR-494 as well as the WDHD1 levels was subsequently determined by means of reverse transcription quantitative polymerase chain reaction (RT-qPCR). After transfection, QBC939 and RBE cell lines were assigned into the blank group (without treatment), the negative control (NC) group (transfected with empty vector), the miR-494 mimic group (transfected with miR-494 mimics), the miR-494 inhibitor group (transfected with miR-494 inhibitors), the sh-WDHD1 group (transfected with shRNA against WDHD1) and the sh-WDHD1 + miR-494 mimic group (transfected with shRNA against WDHD1 and miR-494 mimic).

Twenty-four hours prior to transfection, the cells in each group were inoculated in a 6-well plate (3×10^5 cells/well). In the event that cell confluence reached 80%, the lipofectamine 2000 (Invitrogen, Carlsbad, CA, USA) kit was applied for transfection purposes. Target plasmid and Lipofectamine 2000 were separately diluted using serum-free RPMI 1640 medium (Gibco, USA), gently mixed, permitted to stand at room temperature for 5 min and then blended in an even manner (final concentration 60 nM). After 20 min, the mixture was incubated in a culture plate under 37 °C conditions with 5% CO_2. After 6 h of incubation, the cells were further cultured in new complete medium for 48 h, with the miR-494 mimic and miR-494 inhibitor synthetized by the Shanghai GenePharma Co., Ltd (Shanghai, China), and the shRNA against WDHD1 synthetized by Thermo Fisher software, the sequences of which are displayed in Table 1.

2.5. Cell morphology observation under the inverted microscope

Forty-eight hours post cell transfection, the morphology and EMT of the cells were observed and photographed under an

Table 1
Sequences of miR-494 mimic, inhibitor and sh-WDHD1 for cell transfection.

Plasmid	Sequence
miR-494 mimic	5′-UGA AACAUA CAC GGG AAA CCUC-3′
miR-494 inhibitor	5′-GAGGUU UCC CGU GUA UGU UUC A-3′
sh-WDHD1	5′-GCAATTTGTGGTCTGGCATGG-3′ 5′-CGTTAAACACCAGACCGTACC-3′

Note: miR-494, microRNA-494; WDHD1, WD repeat and high mobility group [HMG]-box DNA-binding protein 1; sh-WDHD1; short hairpin RNA against WDHD1.

inverted microscope. The results revealed a slight increase in cell volume, cell morphology was fusiform or irregular, cell polarity increased, and cell connection was weak. Seventy-two hours post transfection, fluorescent expression was observed under a fluorescence microscope. In the event that the transfection efficiency (fluorescent rate) was over 90%, the subsequent experimentation procedure would be conducted accordingly. Otherwise, the above experiment was repeated.

2.6. Dual luciferase reporter gene assay

The target gene prediction software miRanda was used to predict the miR-494 binding site (UAUGUUUC) of 425–432nt in the 3′-untranslated region (UTR) of WDHD1 mRNA. Dual-luciferase reporter gene assay was employed to verify the target regulation of miR-494 to WDHD1. The wild type (Wt) in the region of WDHD1 mRNA3′-UTR (pWDHD1-wt) and the mutant type of site directed mutagenesis (UAUGUUUC to CGCACCCU) of WT target site (pWDHD1-mut) were synthesized. RBE cells were co-transfected with miR-494 mimic and pWDHD1-wt or with miR-494 mimic and pWDHD1-mut, respectively. The synthetic WDHD1 3′-UTR gene fragments were then inserted into the pMIR-reporter (Huayueyang Biotechnology Co., Ltd., Beijing, China.) at two enzyme sites Spe I and Hind III. A mutation site with a complementary seed sequence was designed in the Wt of WDHD1. The target fragment was then inserted into the pMIR-reporter plasmid using T4 DNA ligase after restriction enzyme digestion. The luciferase reporter plasmids (Wt and Mut) with the correct consequences subsequently co-transfected in a separate manner into HEK-293T cells with miR-494 (CRL-1415, Shanghai Xinyu Biotechnology Co., Ltd., Shanghai, China), respectively. After 48 h of transfection, the cells were collected and lysed. The cells were then centrifuged for 3–5 min followed by collection of the supernatant. Luciferase activity was evaluated using a dual luciferase reporter assay kit (RG005, Beyotime Institute of Biotechnology Co., Ltd, Shanghai, China).

2.7. RT-qPCR

After 48 h of transfection, the QBC939 and RBE cells were collected from each group. The total RNA was extracted from the cell lines using a Trizol assay. RNA integrity was determined using 1% agarose gel electrophoresis, while the RNA concentration and purity were measured using a Nano-Drop ND-1000 spectrophotometer. In accordance with the instructions of EasyScript First-Strand cDNA Synthesis SuperMix (AE301-02, Beijing TransGen Biotech Co., Ltd. Beijing, China), reverse transcription was conducted using a PCR amplification instrument for cDNA template synthesis. Primers for miR-494, U6, WDHD1, E-cadherin, N-cadherin, Vimentin, matrix metalloprotease-9 (MMP-9) and glyceraldehyde-3-phosphate dehydrogenase (GAPDH) were designed and synthesized by Sangon Biotech Co., Ltd. (Shanghai, China) (Table 2). The reverse transcription reaction system was comprised of 20 μL, including 8 μL of total RNA, Anchored Oligo (dT) 18 (0.5 g/L), 10 μL of 2 × ES Reaction Mix and 1 μL of EasyScript RT/RI Enzyme Mix. The reaction liquid was then removed for RT-qPCR. The real time quantitative PCR was performed in accordance with the instructions of the SYBR® Premix Ex TaqTM II kit (Takara Biotechnology Co., Ltd., Dalian, China). The PCR reaction system was comprised of 20 μL, including 10 μL of SYBR Premix, 2 μL of cDNA templates, 0.6 μL of both upstream and downstream primers, 6.8 μL of sterilize water. The real time qPCR was conducted through the application of a fluorescent quantitative PCR instrument (ABI7500, ABI Company, Oyster Bay, NY, USA). U6 was regarded as the internal reference for the detection of miR-494, while GAPDH served as the internal reference for WDHD1, E-cadherin, N-cadherin, Vimentin, Snail, Twist and MMP-9. The reaction conditions were as follows: pre-denaturation at 95 °C for 30 s; denaturation at 95 °C for 30 s, annealing for 20 s and extension at 72 °C for 30 s, for a total of 45 cycles. The expressions of miR-494, U6, WDHD1, E-cadherin, N-cadherin, Vimentin, Snail, Twist, MMP-9 and GADPH were detected. Besides, $2^{-\Delta\Delta Ct}$ indicated a ratio of the target gene expression between the experimental group and the control group, and the formula applied was as follows: $\Delta\Delta CT = \Delta Ct_{\text{the experimental group}} - \Delta Ct_{\text{the control group}}$. The experiment was repeated in triplicate.

Table 2
Primer sequences for reverse transcription quantitative polymerase chain reaction.

Gene	Primer sequence (5′-3′)
miR-494	F: CATAGCCCGTGAAACATACACG R: GTGCAGGGTCCGAGGT
U6	F: GCTTCGGCAGCACATATACTAAAAT R: CGCTTCACGAATTTGCGTGTCAT
WDHD1	F: GCTCGGTCACCCGGTTTTAT R: GGGGCATCATGTCCTCGAAA
E-cadherin	F: TGGAATCCAAGCAGAATTGC R: TATGTGGCAATGCGTTCTCTATCCA
N-cadherin	F: TGTTGCTGCAGAAAACCAAG R: TTTCACAAGTCTCGGCCTCT
Vimentin	F: CGGGATCCGTCCACCAGGTCCGTGTCCTCG R: CCCAAGCTTCTCTTCTTGCAAAGATTCCAC
Snail	F: CCCCAATCGGAAGCCTAACT R: CGTAGGGCTGCTGGAAGGTA
Twist	F: CGGACAAGCTGAGCAAGATT R: CCTTCTCTGGAAACAATGAC
MMP-9	F: ATGTACCCTATGTACCGCTTCACT R: CAGAGAAGAAGAAAAGCTTCTTGG
GAPDH	F: CCACATCGCTCAGACACCAT R: GGCAACAATATCCACTTTACCAGAGT

Note: F: forward; R: reverse; miR-494, microRNA-494; WDHD1 WD repeat and high mobility group [HMG]-box DNA-binding protein 1; MMP-9, matrix metalloprotease-9; GAPDH, glyceraldehyde-3-phosphate dehydrogenase.

2.8. Western blot analysis

After 48-h transfection, the cultured QBC939 and RBE cells in each group were collected, washed with phosphate buffer solution (PBS) and suspended. The cells were then centrifuged followed by extraction of the supernatant. Radioimmunoprecipitation assay (RIPA) lysis buffer (P0013B, Beyotime Institute of Biotechnology Co., Ltd., Shanghai, China) and appropriate amount of phenylmethylsulfonyl fluoride (PMSF) were added to the cells at a ratio of 1×10^7 cells/mL. After re-suspension by means of gentle shaking, the cells were placed over ice for 30 min, centrifuged at 25,764 × *g* for 10 min at 4 °C after which the supernatant was extracted, and regarded as a reflection of the total protein. The protein concentration was determined using a bicinchoninic acid (BCA) kit (Beyotime Institute of Biotechnology Co., Ltd., Shanghai, China) and adjusted to 4 μg/μL using PBS. Cellular total protein (30 μg) was subjected to Sodium Dodecyl Sulfate Polyacrylamide Gel Electrophoresis (SDS-PAGE), transferred onto nitrocellulose membranes by wet process, followed by blockade for 1.5 h in 5% skimmed milk powder formulated with tris-buffered saline plus tween 20 (TBST). The

primary antibodies comprised of the rabbit anti-human WDHD1 (ab72436, 1:2000), E-cadherin (ab40772, 1:100,000), N-cadherin (ab18203, 1:000, 1 ug/mL), Vimentin (ab92547, 1:1000), Twist (ab50581, 1 μg/mL), Snail (ab82846, 1:500), MMP-9 (ab73734, 1:1000, 1 ug/mL), GAPDH (ab9485, 1:2500). All the aforementioned antibodies were purchased from Abcam Inc. (Cambridge, MA, UK). The sealed NC membranes were placed in a plastic dish and incubated with diluted samples of the aforementioned antibodies at 4 °C overnight. The next day, the membranes were rinsed 3 times with TBST (15 min each time). Meanwhile, diluted horseradish peroxidase (HRP)-labeled secondary antibody goat anti-rabbit IgG (ab205718, 1:2000) was incubated at room temperature for 2 h, after which the membranes were rinsed with TBST 3 times (15 min each). Electrochemiluminescence (ECL) luminous liquid was used for coloration, and SmartView Pro 2000 (UVCI-2100, Major, Science, USA) for photography. The Quanity One software was applied for protein band gray scale analysis [15].

2.9. Scratch test

A marker was used to evenly scratch horizontal lines behind a 6 well-plate. After 48-h transfection, QBC939 and RBE cells in each group were incubated with 0.25% trypsin in order to prepare a single cell suspension, after which cell number counting was performed. The cells were inoculated in a 6 well-plate (1×10^6 cells/well), then shaken in a cautious manner and evenly mixed. After 24-h culture in complete medium, the cells were further cultured in the RPMI1640 medium containing 10% FBS. The 6 well-plate was scratched perpendicularly behind the horizontal line using a sterile micro pipette tip (200 μL) followed by three PBS washes. All cells that became detached as a result of the destruction of the pipette tip were removed. The cells were cultured with serum free medium in a 5% CO_2 incubator at 37 °C. Photographs were taken at 0th h and 24th h under a microscope [15].

2.10. Transwell assay

Matrigel (Sigma-Aldrich, St. Louis, MO, USA) was melted overnight at 4 °C, and diluted to a final concentration (1 mg/mL) using pre-cooled serum-free medium at 4 °C (performed on ice). Diluted Matrigel (80 μL/per well) was perpendicularly added to the central part of the apical chamber of Transwell chamber (8 μm of diameter) in order to uniformly distribute the matrix gum, and then cultured at 37 °C for 4 h. After 48 h of transfection, the cells were washed with PBS and serum free medium, respectively, and then suspended with serum-free medium. The number of cells was counted, and the cell concentration was then adjusted to 1×10^6 cells/mL. Next, the basolateral chamber (the bottom of 24 well-plates) was added with 700 μL medium containing 10% serum, and the apical chamber was added with cell suspension. Then, they were cultured for 24 h in an incubator. Tweezers were used to carefully remove the chamber, followed by extraction of the liquid in the apical chamber. At room temperature, following 30-min of fixation in 4% paraformaldehyde, the cells were stained with 0.05% crystal violet for 30 min. The samples were then gently rinsed with water and soaked in several times. The cells in the apical chamber were then carefully removed using wet swabs. The samples were subsequently dried and the number of cells was then counted based on the perspective of 10 random fields selected under an inverted microscope (200×). The experiment was repeated a minimum of 3 times.

2.11. Cell counting kit-8 (CCK-8) assay

After 48-h transfection, QBC939 and RBE cells were washed with PBS twice, detached with 0.25% trypsin and pipetted into single cell suspension. After the cells were counted, they were then inoculated into a 96 well-plate (cell density of 1×10^4 cells per well) with 3 parallel wells. CCK-8 reagent (10 μL) (40203ES60, Shanghai Yeasen Biotechnology Co., Ltd., Shanghai, China) was added into each well after 24-h, 48-h and 72-h culture. After 4 h of incubation, a fully automatic quantitative plotting microplate reader was employed to determine the optical density (OD) value at a wavelength of 450 nm (MK3, Thermo Fisher Scientific, Waltham, MA, USA). A cell viability curve was drawn with the time points as the abscissa and the OD value as the ordinate. The experiment was repeated in triplicate.

2.12. Flow cytometry analysis of propidium iodide (PI) staining

QBC939 and RBE cells were collected after a 48-h period of transfection, prepared into a single cell suspension with 0.25% trypsin, washed twice with PBS and centrifuged for supernatant removal purposes. After centrifugation, the cells were fixed with pre-cooled 70% ethanol at 4 °C overnight, resuspended and then washed with pre-cooled PBS twice. The cells were re-suspended in 100 μL PBS and added with RNase until the final concentration was 1 mg/mL, followed by 30-min water bath at 37 °C. The cells were stained with PI at 4 °C for 40 min under conditions void of light (final concentration 50 μg/mL) and then washed with PBS. The cell cycle DNA content was detected at a wavelength greater than 575 nm, with the percentage of cell cycle calculated.

2.13. Tumor xenograft in nude mice

Thirty specific-pathogen-free (SPF) 5-week-old male BALB/c nude mice (weighted 16–17 g) provided by Beijing Hua Fukang Biological Polytron Technologies Inc (Beijing, China) were recruited for the purposes of the study. The mice were housed in the experimental animal center of Huazhong University of Science and Technology with SPF barrier environment. All bedding, cages, feed and drinking water were sterilized under high temperature or ultraviolet radiation. The temperature was controlled at approximately 25 °C, the air flow rate was 20 cm^3/s, and the air relative humidity was 55%. The nude mice were inoculated with RBE cells in each group with good growth condition. The RBE cells were initially incubated with 0.25% trypsin and washed with PBS 3 times. The cells were then suspended with PBS and gently pipetted in order to construct a single cell suspension. The dorsum of nude mice were inoculated subcutaneously with l00 μL cell suspension (1×10^6) using a 6 gauge needle. The body constitution and growth status of the nude mice were recorded every six days. Thirty days later, the cervical vertebra was dislocated and the nude mice were euthanized. The tumor tissue was resected and preserved for measurement. The tumor volume was obtained using the following formula: 0.5 × long diameter (mm) × short path ^{2}(mm^2). The number of LN metastases was noted. The collected tumor tissues were preserved at −80 °C.

2.14. Statistical analysis

All experimental data were analyzed using SPSS 21.0 software (IBM Corp. Armonk, NY, USA). The measurement data were expressed as mean ± standard deviation. The *t*-test was employed for comparing amongst two groups, while comparisons among multiple groups were performed using one-way analysis of variance (ANOVA), and tested by homogeneity test of variance. In the event the variance analysis was determined to be significantly different, the *q* test was employed for pairwise comparison. The nonparametric rank test was applied when the variance was not uniform. A difference in ($\alpha = 0.05$ was used as a test level) *p value* <0.05 was considered to be statistically significant. Enumeration

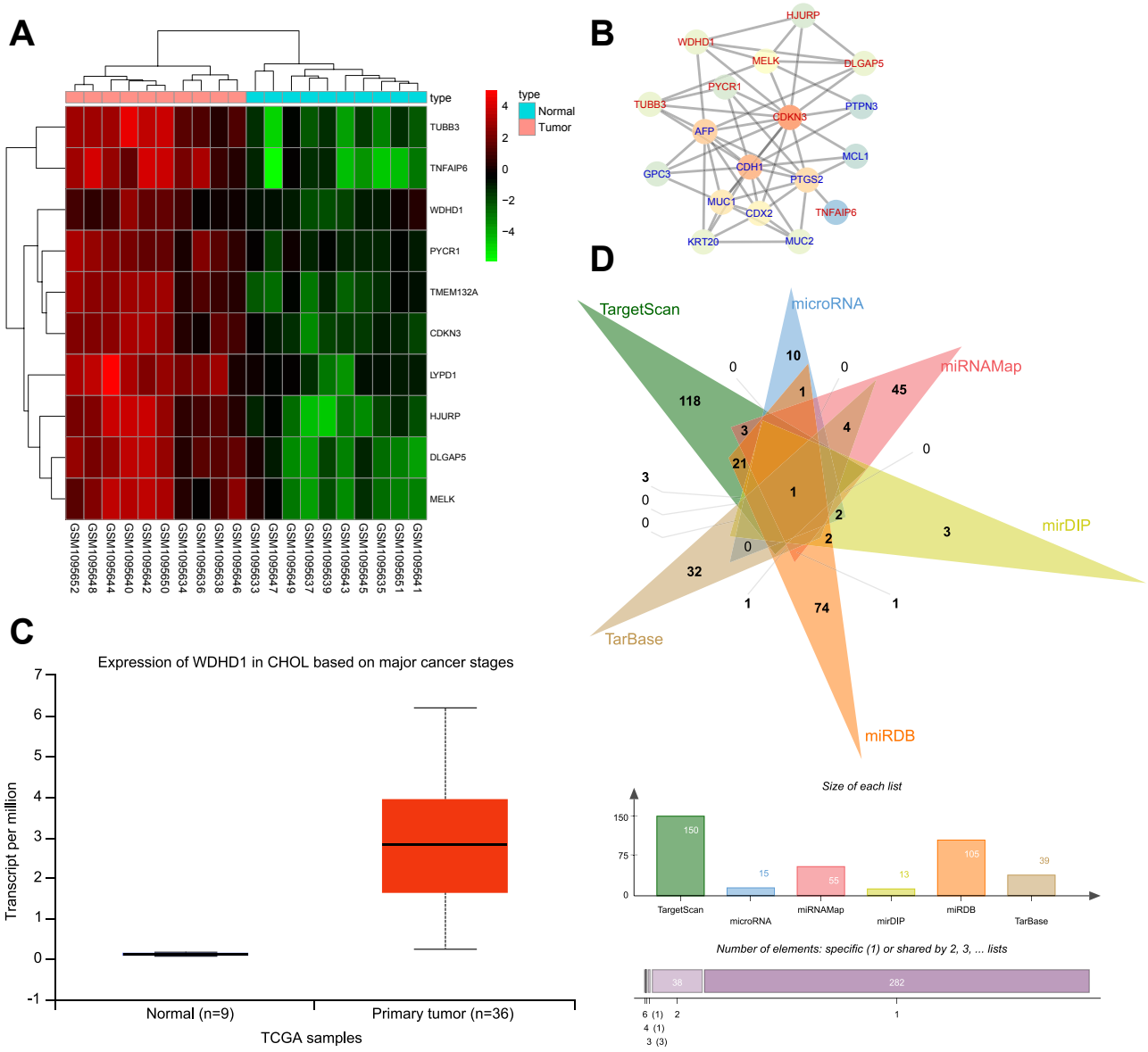

Fig. 1. MiR-494 regulates CCA through WDHD1. (A) Expression histogram of CCA chip GSE45001; X-axis represents sample number and Y-axis represents genes; upward dendrogram represents sample type cluster and vitta connected by dendrogram represents sample type; dendrogram in the left represents gene expression cluster; each cube represents the level of a gene in a sample; upper right color gradation represents gene expression; red is high expression and green is low expression; (B) interactive network between differentially expressed genes and the known genes; each circle represents a gene and its color represents core level of the gene in interactive network; red is in high core level while blue is in low core level; blue words inside the circle represent the known CCA-relative genes and red words represent the obtained differentially expressed genes of CCA; (C) WDHD1 expression in CCA data of TCGA database; X-axis represents sample type and number while Y-axis represents WDHD1 expression; box plot in the left represents normal control sample and box plot in the right is CCA sample; (D) predicted results on regulatory miRNA of WDHD1; different colors represent the intersection of predicted results from different databases; inside figures are the number of miRNAs in this region; histogram below represents included miRNA number from different database; MiR-494, microRNA-494; CCA, cholangiocarcinoma; WDHD1, WD repeat and high mobility group [HMG]-box DNA-binding protein 1; TCGA, The Cancer Genome Atlas.

data were expressed as percentage or ratio, and for comparing amongst values the *chi* square test was used.

3. Results

3.1. MiR-494 plays a regulatory role in CCA through WDHD1

CCA expression chip GSE45001 was retrieved from the GEO database. A total of 2816 differentially expressed genes were obtained through differential analysis of this chip, among which 1426 genes exhibited significantly down-regulated expressions while 1390 genes displayed markedly up-regulated expression levels among the CCA samples. Up-regulated genes in CCA were subjected to the following analysis. Expression thermal maps of 10 obviously elevated genes were constructed (Fig. 1A). In order to further select the CCA-related genes, MalaCards was used to retrieve the known CCA-related genes, with the top 10 genes subsequently selected for the following analysis (Table 3). STRING was employed in order to perform a correlation analysis on the 10 significantly up-regulated genes and the known CCA-related genes (Fig. 1B). The results obtained indicated that CDKN3, WDHD1, MELK, TUBB3 and DLGAP5 were located at a relatively nuclear position and associated with the known CCA-related genes. Further information retrieval on functions of those genes demonstrated that the mechanism of CDKN3, TUBB3, DLGAP5 as well as MELK in tumors had previously been extensively studied, with their relationship already

Table 3
CCA-related genes (top10).

Symbol	Description	Score	PubmedIds
PTPN3	Protein tyrosine phosphatase, non-receptor type 3	454.14	2,450,312,725,075,940
AFP	Alpha fetoprotein	24.79	156,840,082,014,952,000,000,000
MUC1	Mucin 1, cell surface associated	24.04	196,392,171,612,404,000,000,000
MUC2	Mucin 2, oligomeric mucus/gel-forming	23.98	196,392,171,168,059,000,000,000
KRT20	Keratin 20	23.58	190,947,091,572,580,000,000,000
MCL1	MCL1, BCL2 family apoptosis regulator	21.93	159,406,371,223,508,000,000,000
CDH1	Cadherin 1	21.59	18,234,642,176,267,400,000,000
CDX2	Caudal type homeobox 2	21.41	157,258,051,832,996,000,000,000
PTGS2	Prostaglandin-endoperoxide synthase 2	21.24	149,730,681,460,772,000,000,000
GPC3	Glypican 3	21.19	192,126,699,371,521

Notes: CCA, cholangiocarcinoma; PTPN3, protein tyrosine phosphatase, non-receptor type 3; AFP, alpha fetoprotein; MUC1, mucin 1, cell surface associated; MUC2, mucin 2, oligomeric mucus/gel-forming; KRT20, keratin 20; MCL1, BCL2 family apoptosis regulator; CDH1, cadherin 1; CDX2, caudal type homeobox 2; PTGS2, prostaglandin-endoperoxide synthase 2; GPC3, glypican 3.

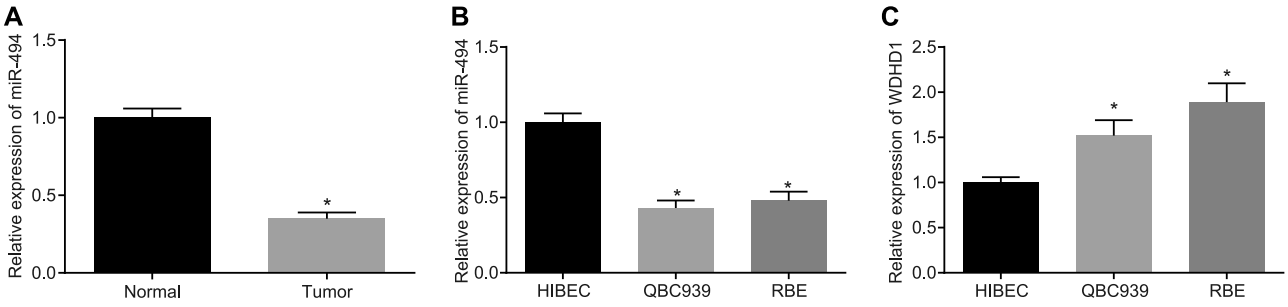

Fig. 2. miR-494 is decreased while WDHD1 exhibited increases in CCA. (A) Relative expression of miR-494 in the normal cholangiocyte tissues (n = 136) and CCA tissues (n = 34); *, $p < 0.05$, vs. the normal cholangiocyte tissues; comparison between two groups is performed using *t* test; (B) relative expression of miR-494 in normal cell line HIBEC and CCA cell lines QBC939 and RBE; (C) relative expression of WDHD1 in normal cell line HIBEC and CCA cell lines QBC939 and RBE; measurement data represent as mean ± SD; the experiment is repeated 3 times; *, $p < 0.05$, vs. normal cell line HIBEC; comparison among multiple groups is analyzed using ANOVA; MiR-494, microRNA-494; CCA, cholangiocarcinoma; WDHD1, WD repeat and high mobility group [HMG]-box DNA-binding protein 1; ANOVA, one-way analysis of variance; SD, standard deviation.

been widely reported [16–20]. However, the reports pertaining to the effect of WDHD1 on tumors were relatively few [11,12] with the related research regarding the effect of WDHD1 on CCA found to be even more rare. In order to further confirm the expression of WDHD1 in CCA, WDHD1 expression in CCA expression data of TCGA was analyzed (Fig. 1C) the results of which showed that in the CCA expression data of TCGA, the WDHD1 level was also elevated. In order to obtain additional information regarding the upstream regulatory mechanism of WDHD1 in CCA, the potential regulatory miRNAs of WDHD1 in TargetScan, microRNA.org and other 3 databases were predicted and the intersection of the predicted results was attained. After that, 744 regulatory miRNAs were found in the TargetScan database and the regulatory miRNAs found in the remaining 5 databases were within 110. Thus, the first 150 miRNAs from the predicted results in the TargetScan database and all predicted miRNAs from the remaining 5 databases were included for analysis purposes followed by the construction of a Venn map (Fig. 1D). The final results revealed that only miR-494 existed in the intersection of the 6 databases, which signified that miR-494 might affect CCA through the regulation of WDHD1.

3.2. miR-494 expression is down-regulated while WDHD1 expression is up-regulated in CCA

RT-qPCR was performed in order to determine the miR-494 expression and level of WDHD1 in both the normal cholangiocyte and CCA tissues. The obtained result indicated that compared with the normal cholangiocyte tissues, there was a marked reduction in the expression of miR-494 in CCA tissues, which further decreased with the progression of CCA (Fig. 2A). In comparison with the normal cholangiocyte cell line HIBEC, miR-494 expression significantly decreased while the WDHD1 level exhibited distinct elevations in cell lines QBC939 and RBE (both $p < 0.05$) (Fig. 2B–C).

Table 4
MiR-494 expression is associated with clinicopathologic features of CCA patients.

Indexes	Cases	Relative expression of miR-494	*p*
Gender			
Male	91	0.358 ± 0.063	0.144
Female	44	0.351 ± 0.063	
Age (years)			
≤60	54	0.354 ± 0.060	0.857
>60	81	0.357 ± 0.065	
Tumor size (cm)			
≤5	72	0.359 ± 0.058	0.584
>5	63	0.353 ± 0.069	
Lymph node metastasis			
With	41	0.282 ± 0.040	<0.001
Without	94	0.388 ± 0.040	
Distant metastasis			
With	35	0.274 ± 0.038	<0.001
Without	100	0.384 ± 0.041	
TNM stage			
I–II	39	0.280 ± 0.040	<0.001
III–IV	96	0.359 ± 0.063	

Notes: MiR-494, microRNA-494; CCA, cholangiocarcinoma; TNM, tumor node metastasis.

Taken together, based on the results obtained it was concluded that miR-494 was expressed poorly while WDHD1 was highly expressed in CCA.

3.3. MiR-494 is expressed poorly with lymph node metastasis and distant metastasis as well as at TNM III–IV stage of CCA

Next, the relationship between miR-494 expression and clinicopathologic features of CCA patients was measured. The results (Table 4) revealed that miR-494 expression was irrelevant in regard to the parameters of age, gender and tumor

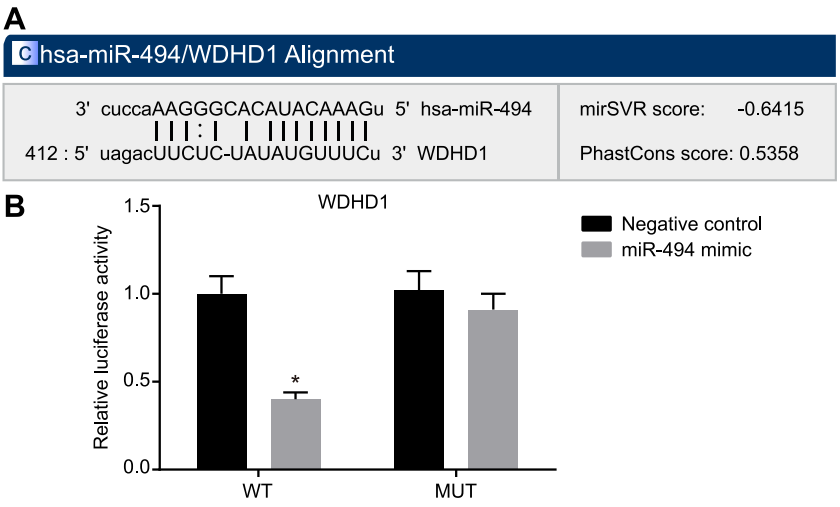

Fig. 3. Bioinformatics prediction and dual-luciferase reporter gene assay reveal that WDHD1 is a target gene of miR-494. (A) The binding sites of miR-494 to WDHD1 predicted by bioinformatics software; (B) WDHD1 is verified as a target gene of miR-494 by dual luciferase reporter gene activity assay; measurement data represent as mean ± SD; the experiment is repeated 3 times; *, $p < 0.05$, vs. the NC group; comparison between two groups is performed using *t* test; WDHD1, WD repeat and high mobility group [HMG]-box DNA-binding protein 1; WT, wild type; MUT, mutant type; NC, negative control; miR-494, microRNA-494; SD, standard deviation.

size (all $p > 0.05$) while correlations to lymph node metastasis, distant metastasis and TNM stage were established (all $p < 0.05$). Besides, these findings also demonstrated that miR-494 expression was relatively lower with lymph node metastasis and distant metastasis as well as at TNM III–IV stage of CCA.

3.4. MiR-494 binds to WDHD1 in its 3′UTR

Initially, bioinformatics prediction using miRanda software (microRNA.org) and dual-luciferase reporter gene assay were performed in order to identify the relationship between miR-494 and WDHD1. The results of bioinformatics prediction demonstrated that WDHD1 was indeed a target gene of miR-494 (Fig. 3A). The results of dual-luciferase reporter gene assay (Fig. 3B) revealed that luciferase activity was prominently reduced when co-transfection with miR-494 mimic and pWDHD1-wt ($p < 0.05$). No significant difference was detected regarding luciferase activity in the cells co-transfected with miR-494 mimic and pWDHD1-mut ($p > 0.05$). These findings demonstrated that miR-494 could specifically bind to the WDHD1 gene.

3.5. The miR-494 improves cell morphology and modulates EMT-specific markers by negatively regulating WDHD1

Initially, cell volume and morphology were detected, the results of which disclosed that compared with the blank and NC groups, cells in the miR-494 inhibitor group were swollen, spindle-shaped, irregular, polarized, and detached, while cells in the miR-494 mimic group, si-WDHD1 group and sh-WDHD1 + miR-494 mimic groups were round-shaped and closely conjunct (Fig. 4).

RT-qPCR and western blot analysis methods were subsequently employed in order to further investigate the mechanism by which miR-494 influences the expression patterns of E-cadherin, WDHD1, N-cadherin, Vimentin and MMP-9. As illustrated in Fig. 5, the mRNA and protein levels of related factors were similar in cell lines QBC939 and RBE of the NC and blank groups (all $p > 0.05$). In comparison with the NC and blank groups, expression of miR-494 was up-regulated in the miR-494 mimic group ($p < 0.01$), while the expression was detected to be down-regulated in the miR-494 inhibitor group ($p < 0.05$). No significant difference was observed in relation to the expression of miR-494 among the NC and blank, sh-WDHD1 groups ($p > 0.05$), with identical observations made between the miR-494 mimic and sh-WDHD1 + miR-494 mimic groups ($p > 0.05$). In comparison to the NC and blank groups, mRNA and protein expression of E-cadherin was up-regulated in the miR-494 mimic and sh-WDHD1 groups (both $p < 0.05$), while that of WDHD1, N-cadherin, Vimentin, Snail, Twist and MMP-9 was remarkably reduced (all $p < 0.05$). The miR-494 inhibitor group exhibited decreased mRNA and protein expressions of E-cadherin yet remarkably increased mRNA and protein expressions of WDHD1, N-cadherin, Vimentin, Snail, Twist and MMP-9 than the NC and blank groups (all $p < 0.05$). The mRNA and protein expression of E-cadherin was elevated while the mRNA and protein expressions of WDHD1, N-cadherin, Vimentin, Snail, Twist and MMP-9 were remarkably reduced in the sh-WDHD1 + miR-494 mimic group compared to the miR-494 mimic group (all $p < 0.05$). Based on the aforementioned results, it was concluded that overexpressed miR-494 could increase mRNA and protein expression of E-cadherin while acting to decrease the mRNA and protein expressions of WDHD1, N-cadherin, Vimentin, Snail, Twist and MMP-9.

3.6. Inhibition of WDHD1 by overexpressed miR-494 reduces cell migration and invasion of CCA

A scratch test was performed in order to demonstrate the effect of miR-494 on CCA cell migration. The results (Fig. 6) revealed that the cell migration of cell lines QBC939 and RBE in the miR-494 mimic and sh-WDHD1 groups was markedly lower at 24th h compared with the blank and NC groups at the same time point ($p < 0.05$), while cell migration in the sh-WDHD1 + miR-494 mimic group evidently decreased at 24th h ($p < 0.01$). However, the cell migration in the miR-494 inhibitor group was unmistakably higher at 24th h than the blank and NC groups at the same time point ($p < 0.05$). No significant difference was observed regarding cell migration between the blank and NC group ($p > 0.05$), between the miR-494 mimic and sh-WDHD1 group ($p > 0.05$). These findings demonstrated that miR-494 overexpression could potentially decelerate cell migration of CCA.

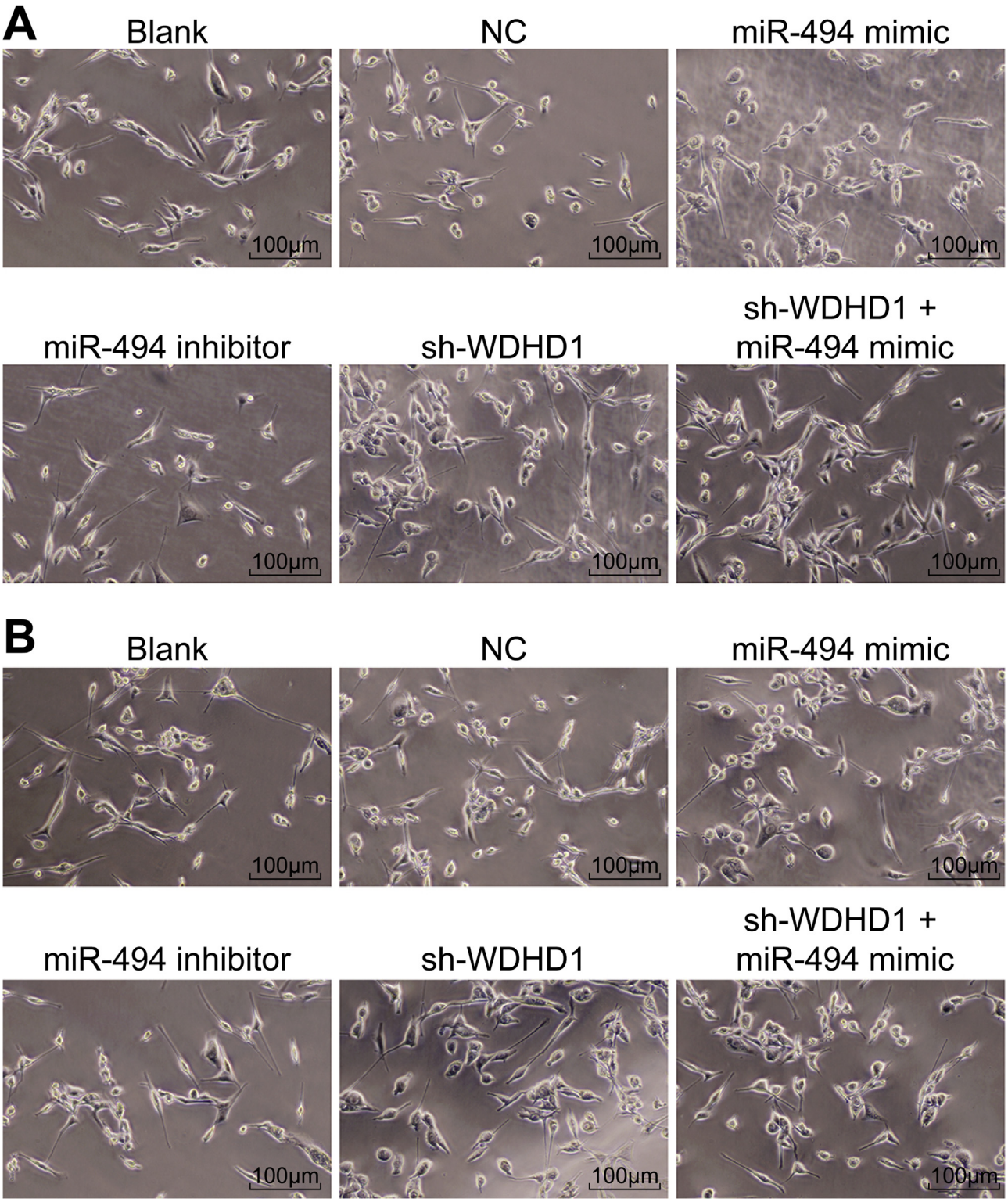

Fig. 4. Cell morphology is captured under the inverted microscope, showing miR-494 depletion correlates to the occurrence of EMT. (A) morphology change of cell line QBC939 (×100); (B) morphology change of cell line RBE (×100); miR-494, microRNA-494; EMT, epithelial-mesenchymal transition.

Next, the effects of miR-494 on CCA cell invasion were analyzed using Transwell assay. The results as indicated in Fig. 7 suggested similar cell invasion in cell lines QBC939 and RBE in the NC and blank groups ($p > 0.05$). In comparison to the blank and NC groups, the number of invaded cells in the miR-494 mimic and sh-WDHD1 groups evidently reduced ($p < 0.05$), while that in the miR-494 inhibitor group was obviously increased ($p < 0.05$). The number of invaded cells was found to have dramatically diminished in the sh-WDHD1 + miR-494 group when compared to the miR-494 mimic and sh-WDHD1 groups ($p < 0.05$). No significant difference was observed in the cell invasion between the sh-WDHD1 and miR-494 mimic groups ($p > 0.05$). The above findings suggested that miR-494 overexpression could result in reduced cell invasion of CCA.

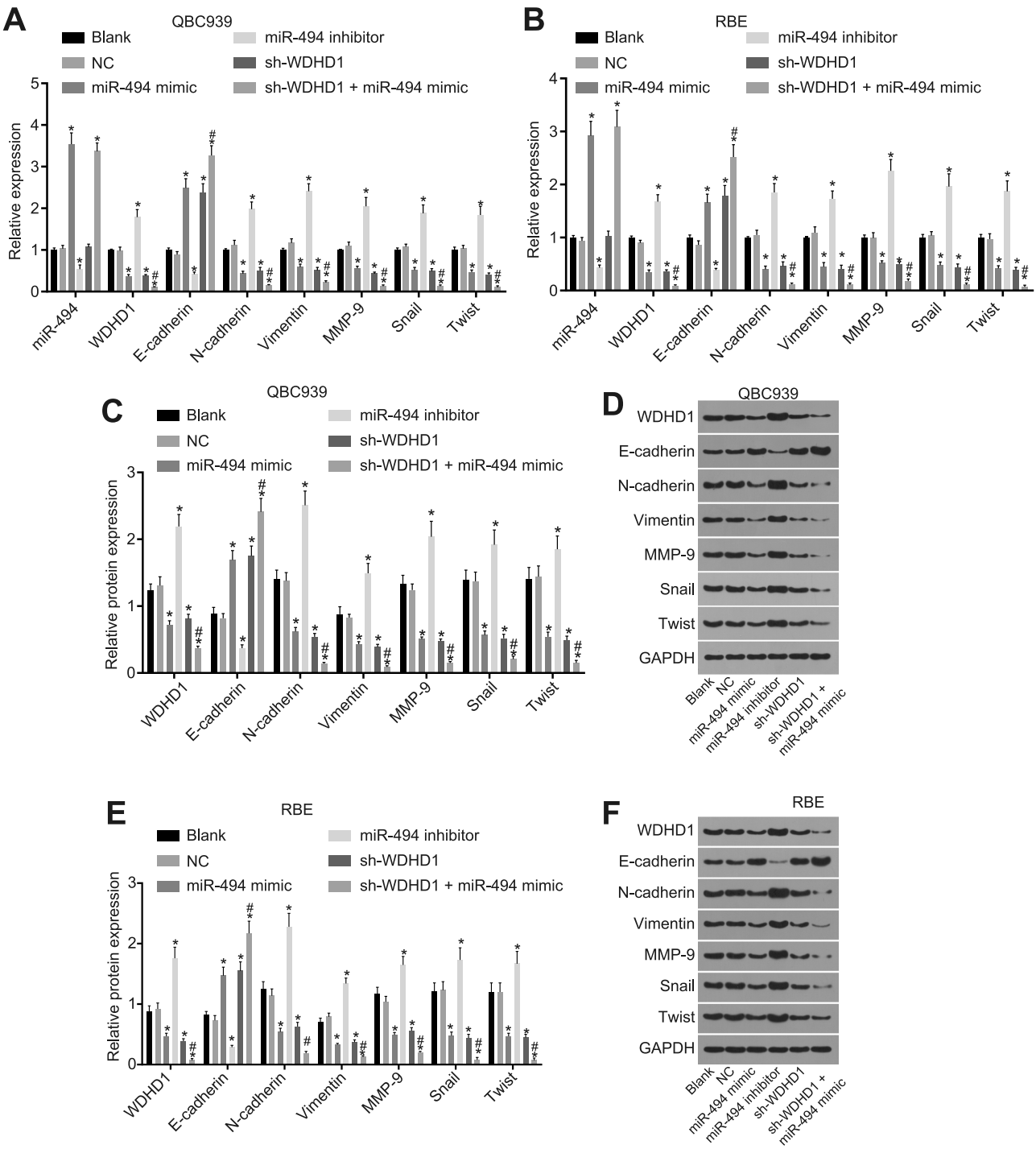

Fig. 5. MiR-494 negatively regulates WDHD1 and modulates EMT-specific markers. (A) mRNA expressions of WDHD1, E-cadherin, N-cadherin, Vimentin, Snail, Twist and MMP-9 in cell line QBC939 detected by RT-qPCR; (B) mRNA expressions of WDHD1, E-cadherin, N-cadherin, Vimentin, Snail, Twist and MMP-9 in cell line RBE detected by RT-qPCR; (C) protein expressions of WDHD1, E-cadherin, N-cadherin, Vimentin, Snail, Twist and MMP-9 in cell line QBC939 measured by western blot analysis; (D) protein bands of WDHD1, E-cadherin, N-cadherin, Vimentin, Snail, Twist and MMP-9 in cell line QBC939 detected by western blot analysis; (E) protein expressions of WDHD1, E-cadherin, N-cadherin, Vimentin, Snail, Twist and MMP-9 in cell line RBE9 detected by western blot analysis; (F) protein bands of WDHD1, E-cadherin, N-cadherin, Vimentin, Snail, Twist and MMP-9 in cell line RBE detected by western blot analysis; measurement data represent as mean ± SD; the experiment is repeated 3 times; *, $p < 0.05$, vs. the blank group; #, $p < 0.05$, vs. the miR-494 mimic group; comparison among multiple groups is analyzed using ANOVA; RT-qPCR, reverse transcription quantitative polymerase chain reaction; miR-494, microRNA-494; WDHD1, WD repeat and high mobility group [HMG]-box DNA-binding protein 1; NC, negative control; MMP, matrix metalloproteinase; ANOVA, one-way analysis of variance; SD, standard deviation.

3.7. Overexpressed miR-494 represses cell viability via WDHD1 inhibition with dosage-dependent effect

In order to determine whether miR-494 had a dosage-dependent effect on CCA cell growth, cell lines QBC939 and RBE were transfected with miR-494 mimic plasmid (20 nM, 40 nM and 60 nM) for 72 h. The results demonstrated that (Fig. 8A–B) in comparison with the control group (0 nM), the group transfected with miR-494 mimic plasmid significantly inhibited cell

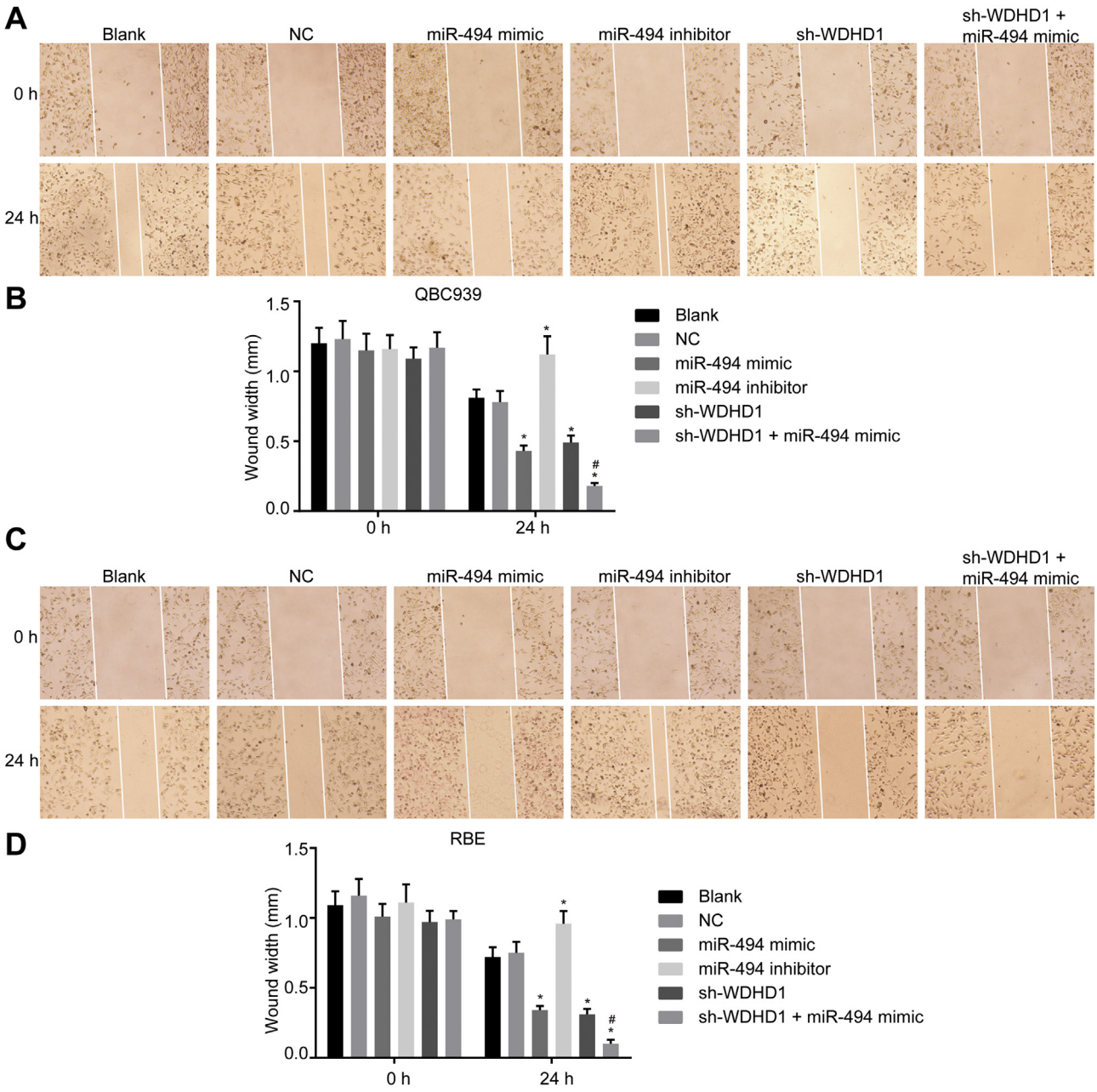

Fig. 6. Overexpressed miR-494 decreases cell migration in cell lines QBC939 and RBE by inhibiting WDHD1. (A) Cell scratch results of cell line QBC939 in each group (×100); (B) cell migration results of cell line QBC939 in each group; (C) cell scratch results of cell line RBE in each group (×100); (D) cell migration results of cell line RBE in each group; measurement data represent as mean ± SD; the experiment is repeated 3 times; *, $p < 0.05$, vs. the blank group,; #, $p < 0.05$, vs. the miR-494 mimic group; comparison among multiple groups is analyzed using ANOVA; miR-494, microRNA-494; WDHD1, WD repeat and high mobility group [HMG]-box DNA-binding protein 1; NC, negative control; ANOVA, one-way analysis of variance; SD, standard deviation.

growth in QBC939 and RBE, due to a dosage-dependent effect ($p > 0.05$).

A CCK-8 assay was subsequently utilized to demonstrate the modulation of miR-494 on CCA cell viability. As displayed in Fig. 8C–D, the OD value in cell lines QBC939 and RBE in the blank group was similar to the value observed in the NC group after 24-h, 48-h and 72-h of incubation ($p > 0.05$). The OD value of the miR-494 inhibitor group was higher when compared to the value of the blank group ($p < 0.05$), suggesting there was an increase in cell viability and proliferation rate. In the miR-494 mimic and sh-WDHD1 groups, the OD value was decreased than the blank group ($p < 0.05$) suggesting inhibited cell viability and proliferation rate. In comparison to the miR-494 mimic and sh-WDHD1 groups, the OD value significantly declined in the sh-WDHD1 + miR-494 mimic group ($p < 0.05$), suggesting inhibited cell viability and proliferation rate. No significant difference was observed in the OD value between the sh-WDHD1 group and the miR-494 mimic group ($p > 0.05$). The above findings indicated that miR-494 overexpression could inhibit CCA cell viability with a dosage-dependent effect.

3.8. Overexpressed miR-494 decreases cell cycle progression via WDHD1 inhibition

Next, flow cytometry was performed in order to examine the impacts of miR-494 on CCA cell cycle distribution. In cell lines

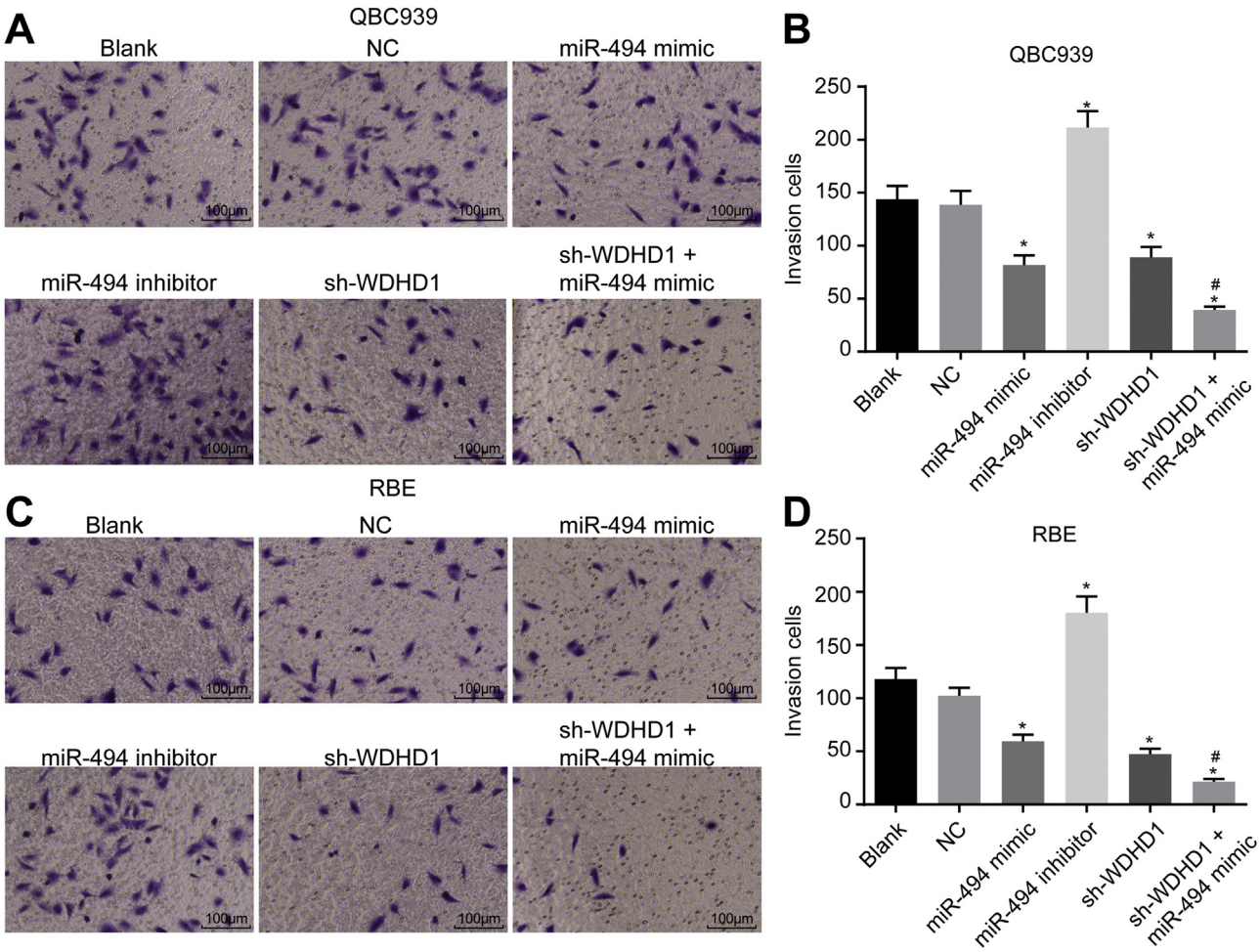

Fig. 7. Overexpressed miR-494 reduces cell invasion in cell lines QBC939 and RBE by suppressing WDHD1 detected by Transwell assay. (A) Cell invasion results in cell line QBC939 at 24 h after transfection (×100); (B) the number of invaded cells in cell line QBC939 at 24 h after transfection; (C) the cell invasion in cell line RBE at 24 h after transfection (×100); (D) the number of invaded cells in cell line RBE at 24 h after transfection; measurement data represent as mean ± SD; the experiment is repeated 3 times; *, $p < 0.05$, vs. the blank group; #, $p < 0.05$, vs. the miR-494 mimic group; comparison among multiple groups is analyzed using ANOVA; miR-494, microRNA-494; WDHD1, WD repeat and high mobility group [HMG]-box DNA-binding protein 1; NC, negative control; ANOVA, one-way analysis of variance; SD, standard deviation.

QBC939 and RBE, no difference was observed in the proportion of cell cycle phases between the blank and NC groups ($p > 0.05$). In comparison with the blank group and the NC group, the percentage of cells at the G1 phase was significantly raised, while the percentage of cells at the S phase was significantly decreased in the miR-494 mimic and sh-WDHD1 groups (both $p < 0.05$). In the miR-494 inhibitor group, the percentage of cells at the G1 phase was significantly reduced, while the percentage of cells at the S phase was significantly elevated compared to the blank and NC groups (both $p < 0.05$). No significant difference was observed regarding the proportion of cell cycle phases between the miR-494 mimic group and the sh-WDHD1 group ($p > 0.05$). On comparing with the miR-494 mimic group, it was observed that the percentage of cells at G1 phase significantly enhanced, while the percentage of cells at the S phase notably reduced in the sh-WDHD1 + miR-494 mimic group (both $p < 0.05$) (Fig. 9). It was ultimately concluded that miR-494 overexpression might contribute to cell cycle arrest of CCA.

3.9. Overexpressed miR-494 protects nude mice against tumor formation

During the in vivo experiment, the role of miR-494 in tumor formation was assessed among the recruited nude mice. The results of BALB/c tumor-formation in nude mice (Fig. 10) provided evidence indicating that after 30 days of inoculation, there was no difference in tumor-formation ability between the blank and NC groups ($p > 0.05$). In comparison to the blank and NC groups, the tumor forming ability of cell line RBE and the volume of tumor nodules were obviously diminished in the miR-494 mimic and sh-WDHD1 groups ($p < 0.05$) suggesting inhibited tumor growth; while in the miR-494 inhibitor group, the ability of tumor-formation and the volume of tumor nodules were evidently raised ($p < 0.05$). In comparison with the miR-494 mimic and sh-WDHD1 groups, the ability of tumor-formation and the volume of tumor nodules were significantly downregulated in the sh-WDHD1 + miR-494 mimic group ($p < 0.05$). No significant difference was detected in relation to the tumor-formation ability between the miR-494 mimic and sh-WDHD1 groups ($p > 0.05$). It was ultimately concluded based on the aforementioned findings that overexpressed miR-494 protects nude mice against tumor formation.

4. Discussion

CCA represents a rare tumor form that is accompanied by a poor prognosis [21]. EMT has been hypothesized as a major mechanism contributing to the metastasis of CCA [22]. LNM has been widely reported to function as a significant prognostic factor in ICCA [23]. Current literature has provided evidence highlighting the urgency behind the need to adequately define the underlying mechanisms associated with the malignant behavior of CCA, which could help

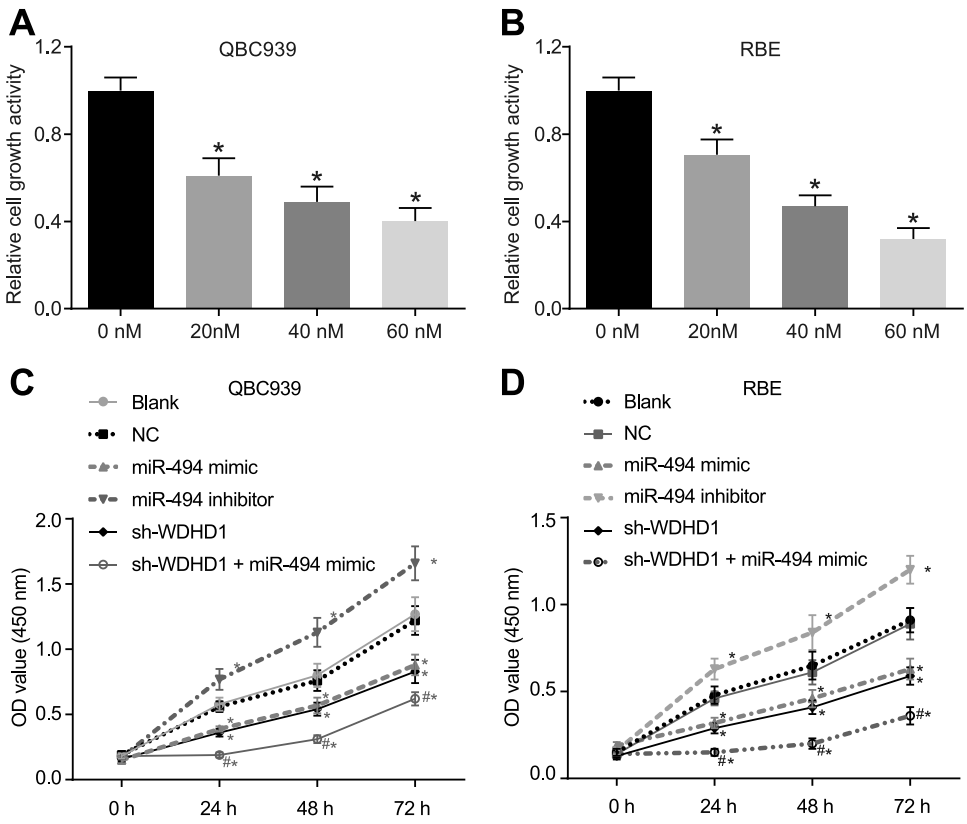

Fig. 8. Overexpressed miR-494 represses cell viability *via* WDHD1 inhibition in cell lines QBC939 and RBE detected by CCK-8 assay. (A) Cell viability in cell line QBC939 transfected with miR-494 mimic of concentration 0 nM, 20 nM, 40 nM and 60 nM; (B) cell viability in cell line RBE transfected with miR-494 mimic of concentration 0 nM, 20 nM, 40 nM and 60 nM; *, $p < 0.05$, vs. the 0 nM group; (C) growth curve of cell line QBC939 in each group at 0 h, 24 h, 48 h and 72 h; (D) growth curve of cell line RBE in each group at 0 h, 24 h, 48 h and 72 h; measurement data represent as mean ± SD; the experiment is repeated 3 times; *, $p < 0.05$, vs. the blank group; #, $p < 0.05$, vs. the miR-494 mimic group; comparison among multiple groups is analyzed using ANOVA; CCK-8, cell counting kit-8; miR-494, microRNA-494; WDHD1, WD repeat and high mobility group [HMG]-box DNA-binding protein 1; NC, negative control; ANOVA, one-way analysis of variance; SD, standard deviation.

enhance the development of more effective clinical strategies [24]. A previous study reported decreased miR-494 in human CCA cells, while a recent landmark finding revealed the function of miRNAs on binding specificity to their targets [9]. Dual luciferase reporter gene assay provided verification indicating that WDHD1 is a target gene of miR-494 in the current study. Meanwhile, evidence was obtained demonstrating that miR-494 binding to WDHD1 may prevent CCA progression through its down-regulated role in EMT and LNM.

Initially, bioinformatics prediction was applied by using microRNA.org, which revealed that miR-494 could target WDHD1. A key observation in the present study showed that cells treated with WDHD1 silencing or miR-494 overexpression exhibited descended expressions of WDHD1, N-cadherin, Vimentin and MMP-9, along with ascended expressions of E-cadherin. EMT has been determined to be powerful process associated with the invasion, metastasis and tumorigenicity of tumors; thankfully, evidence has been presented indicating that miRNAs can play an essential role in regulating EMT in cancer progression [25]. Correspondingly, studies have shown that miRNA expression is closely related to the biological and clinical behavior of ICCA [8]. During the present study, we also identified that miR-494 regulated the expressions of EMT-related genes, and inhibit EMT in CCA cells. Besides, EMT-related genes including E-cadherin, Ncadherin, vimentin, MMP-2, and MMP-9, have been reported to play central roles in cancer cellular motility, invasiveness and metastasis during tumorigenesis [26]. In lung cancer cells, the overexpression of miR-23a has been suggested to be capable of suppressing E-cadherin expression and stimulating EMT [27]. Consistently, through the suppression of N-cadherin and EMT, miR-145-5p could suppress the metastatic capacity and invasion of gastric cancer (GC) cells [28]. Upregulation of miR-138 in renal cell carcinoma (RCCA) cell lines has been shown to suppress the expression pattern of vimentin [29]. The expression of MMP-2 and MMP-9 descended following transfection with miR-138, and ascended after transfection with miR-138 inhibitor in CCA cells [30]. WDHD1 was originally identified by means of screening for mutant genes affecting chromosome transmission fidelity, and was noted to be overexpressed in cases of lung cancers and esophageal cancer [11]. Its knockdown can impair the growth and viability of acute myeloid leukemia (AML) cells [31], which is in line with our results. Depression of WDHD1 induces cell cycle progression deficiencies due to defective centromere [32].

In order to further analyze the regulation of miR-494 targeting WDHD1 in the development of CCA, sh-WDHD1 or miR-494 mimic was introduced into cells, the results of which demonstrated suppressed migration, invasion and viability in CCA cells, while its cell cycle progression was blocked by miR-494 mediating WDHD1. Besides, miR-494-3p has been reported to target CXCR4 resulting in the restraint of various biological processes including proliferation, invasion, and migration of prostate cancer cells [33]. Furthermore, miR-494 has previously been identified as a potential prognostic marker in epithelial ovarian cancer, and its target SIRT1 to inhibit cellular proliferation, migration and invasion [34]. A previous study proposed the functionality of miR-494 in modulating modulate multiple molecules involved in the canonical G1-S transition, as well as various molecules related to process of the G2/M transition [9]. Consistently, functional study concluded that overexpressed miR-494 could contribute to the induction of pancreatic cancer (PC) cells at the G1 phase [35]. Reports have suggested that miR-494 is

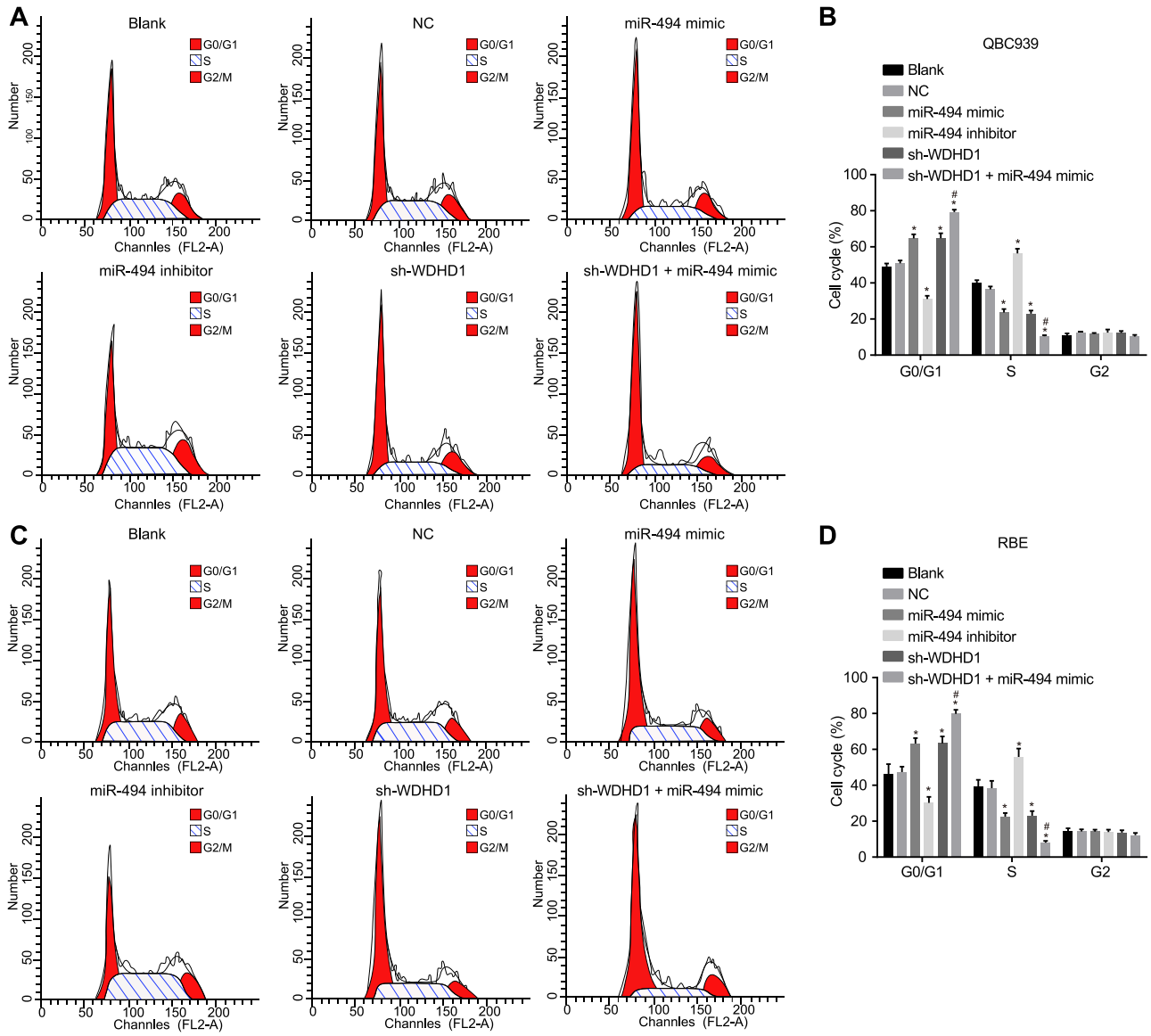

Fig. 9. MiR-494 overexpression decreases cell cycle progression *via* WDHD1 inhibition in cell lines QBC939 and RBE. (A) The percentage of G2, S and G1 phase in cell line QBC939 after transfection shown by flow cytometry; (B) cell cycle distribution in cell line QBC939 after transfection; (C) the percentage of G2, S and G1 phase in cell line RBE after transfection was shown by flow cytometry; (D) cell cycle distribution in cell line RBE after transfection; measurement data represent as mean ± SD; the experiment is repeated 3 times; *, $p < 0.05$ vs. the blank group; #, $p < 0.05$, vs. the miR-494 mimic group; comparison among multiple groups is analyzed using ANOVA; miR-494, microRNA-494; WDHD1, WD repeat and high mobility group [HMG]-box DNA-binding protein 1; NC, negative control; ANOVA, one-way analysis of variance; SD, standard deviation.

expressed at a low level in human CCA cells, and miR-494 reinforcement leads to cancer growth inhibition, in part through reinforcing the G1-S transition checkpoint. [9]. Meanwhile, an association was observed between positive WDHD1 expression and poor prognosis in non-small cell lung cancer [11]. Furthermore, the depletion of WDHD1 has been revealed to increase DNA damage, resulting in the accumulation of late S- and/or G2-phase cells [36]. Prior to the culmination of the present study, in vivo experiments were performed, the results of which indicated that overexpressed miR-494 or WDHD1 silencing suppressed tumor formation as well as LNM, ultimately providing further verification in relation to the findings regarding miR-494 functioning as a tumor suppressor in CCA in the present study.

Besides, a large array of signaling pathways have been demonstrated to participate in regulating EMT of tumor cells, such as involvement of activated TGF-β in EMT of tumors [37] and inhibition of EMT of tumor cells through the regulation of MAPK in the Akt-MDM2-Foxo3A signaling pathway [38]. As the homologous gene of Cgf4/mcl1, WDHD1 mainly participates to regulate cell DNA replication and division cycle. Nagato Sato highlighted aberrantly activated WDHD1 in lung and esophageal carcinomas and provided evidence verifying that WDHD1 expression might influence tumor formation and progression of lung and esophageal cancer by serving as a downstream molecule and a cell cycle regulator in the phosphoinositide 3-kinase/AKT pathway [11]. However, the specific downstream signaling pathway of WDHD1 in CCA remains largely unclear.

A previous study involving CCA cell lines QBC939 and RBE for biological investigative purposes revealed that the expression of a certain factor in cells was interfered or overexpressed to explore the changes of the biological function of the cells. For example, the inhibition of p53 expression in CCA cell lines QBC939 and RBE has been found to inhibit autophagy, which acts to ultimately enhance the chemosensitivity of QBC939 and RBE with nutritional deficiency

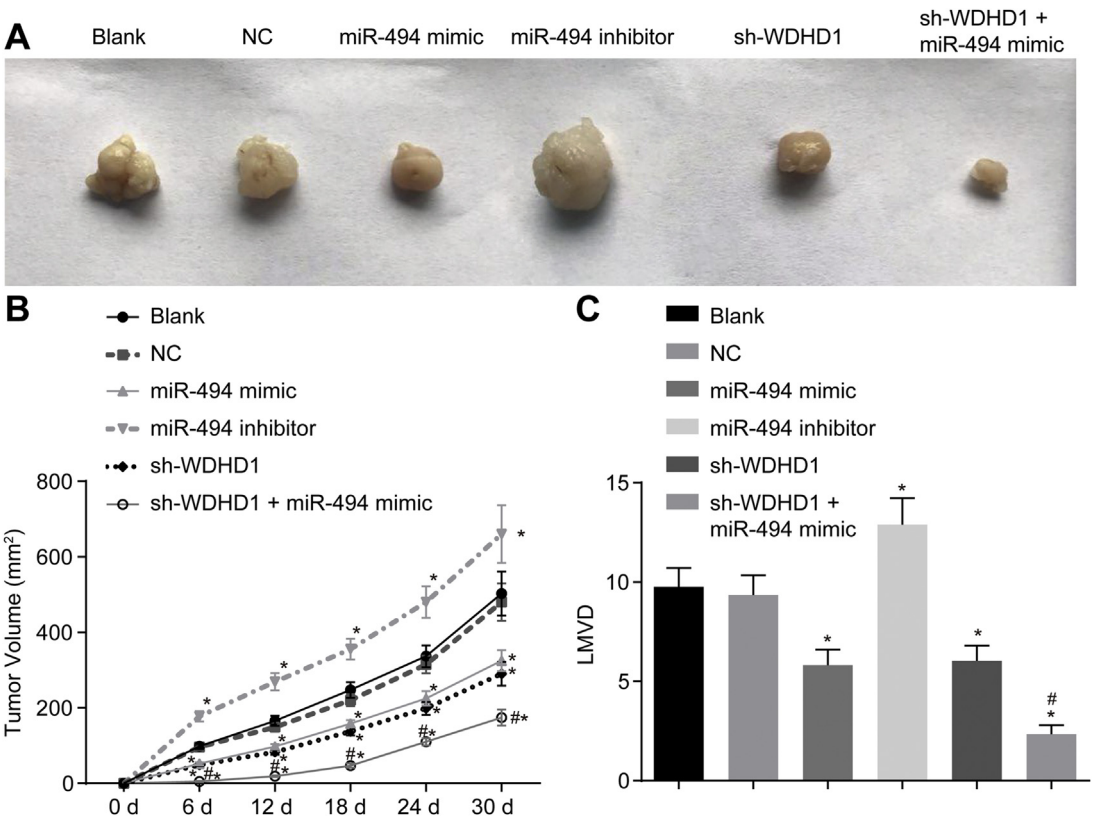

Fig. 10. Overexpressed miR-494 protects nude mice against tumor formation and LNM. (A) Tumor xenografts in nude mice of each group; (B) tumor volume change in nude mice of each group; (C) the number of LNM in nude mice of each group; *, $p < 0.05$, vs. the blank group; #, $p < 0.05$, vs. the miR-494 mimic group; measurement data represent as mean ± SD; the experiment is repeated 3 times; comparison among multiple groups is analyzed using ANOVA; miR-494, microRNA-494; WDHD1, WD repeat and high mobility group [HMG]-box DNA-binding protein 1; LNM, lymph node metastasis; ANOVA, one-way analysis of variance; SD, standard deviation.

[39]. Reports have suggested that overexpression or silencing of miR-21 in CCA cell line QBC939 and RBE can regulate EMT of CCA cells [40]. Furthermore, a previous study highlighted the role of overexpressed miR-122 in the inhibition of the proliferation, invasion and apoptosis of human cholangiocarcinoma cells was verified in CCA QBC939 and RBE cell lines [41]. During the current study, the miR-494 and WDHD1 expression was influenced in the CCA cell line QBC939 and RBE simultaneously in an attempt to explore the changes of EMT and LNM of CCA, with the results of the two cell lines found to be largely consistent: indicating that miR-494 inhibited EMT and LNM of CCA cells by down-regulating WDHD1.

In conclusion, our study demonstrated that miR-494 inhibited EMT and LNM in CCA cells by targeting WDHD1, thus highlighting a promising target in the treatment for CCA. Furthermore, miR-494 was indicated as a tumor suppressor in CCA implicated in the regression of CCA cell progression, and activities such as viability, migration, and invasion. Our study ultimately presents a valuable therapeutic strategy through the upregulation of miR-494 in patients suffering from CCA. However, the current study only presents the theoretical basis of this mechanism in CCA cells. Therefore, clinical experiments of fully developed miR-based anti-cancer therapeutic agent should be perfected in the future. Moreover, further research is required in order to explore the specific mechanism especially the comprehensive impacts of miR-494 on various molecules as well as signaling pathways involved in the occurrence and development of CCA.

Conflict of interest

None declared.

Acknowledgement

This work was supported by the Natural Science Foundation of Hunan Province (2018JJ2564).

References

[1] Razumilava N, Gores GJ. Cholangiocarcinoma. Lancet 2014;383:2168–79.
[2] Arai Y, Totoki Y, Hosoda F, Shirota T, Hama N, Nakamura H, et al. Fibroblast growth factor receptor 2 tyrosine kinase fusions define a unique molecular subtype of cholangiocarcinoma. Hepatology 2014;59:1427–34.
[3] Tyson GL, El-Serag HB. Risk factors for cholangiocarcinoma. Hepatology 2011;54:173–84.
[4] Razumilava N, Gores GJ. Classification, diagnosis, and management of cholangiocarcinoma. Clin Gastroenterol Hepatol 2013;11, 13-21.e1; quiz e3-4.
[5] Valle JW, Borbath I, Khan SA, Huguet F, Gruenberger T, Arnold D. Biliary cancer: ESMO Clinical Practice Guidelines for diagnosis, treatment and follow-up. Ann Oncol 2016;27:v28–37.
[6] Charbel H, Al-Kawas FH. Cholangiocarcinoma treatment. Curr Gastroenterol Rep 2012;14:528–33.
[7] Aljiffry M, Abdulelah A, Walsh M, Peltekian K, Alwayn I, Molinari M. Evidence-based approach to cholangiocarcinoma: a systematic review of the current literature. J Am Coll Surg 2009;208:134–47.
[8] Yang R, Chen Y, Tang C, Li H, Wang B, Yan Q, et al. MicroRNA-144 suppresses cholangiocarcinoma cell proliferation and invasion through targeting platelet activating factor acetylhydrolase isoform 1b. BMC Cancer 2014;14:917.
[9] Yamanaka S, Campbell NR, An F, Kuo SC, Potter JJ, Mezey E, et al. Coordinated effects of microRNA-494 induce G(2)/M arrest in human cholangiocarcinoma. Cell Cycle 2012;11:2729–38.
[10] Olaru AV, Ghiaur G, Yamanaka S, Luvsanjav D, An F, Popescu I, et al. MicroRNA down-regulated in human cholangiocarcinoma control cell cycle through multiple targets involved in the G1/S checkpoint. Hepatology 2011;54:2089–98.
[11] Sato N, Koinuma J, Fujita M, Hosokawa M, Ito T, Tsuchiya E, et al. Activation of WD repeat and high-mobility group box DNA binding protein 1 in pulmonary and esophageal carcinogenesis. Clin Cancer Res 2010;16:226–39.
[12] Zhou Y, Zhang Q, Gao G, Zhang X, Liu Y, Yuan S, et al. Role of WDHD1 in human papillomavirus-mediated oncogenesis identified by transcriptional profiling of E7-expressing cells. J Virol 2016;90:6071–84.

[13] Higuchi R, Yamamoto M, Hatori T, et al. Intrahepatic cholangiocarcinoma with lymph node metastasis successfully treated by immunotherapy with CD3-activated T cells and dendritic cells after surgery: report of a case. Surg Today 2006;36:559–62.
[14] Imajyo I, Sugiura T, Kobayashi Y, Shimizu K, Imai K, Takasaki K. T-box transcription factor Brachyury expression is correlated with epithelial-mesenchymal transition and lymph node metastasis in oral squamous cell carcinoma. Int J Oncol 2012;41:1985–95.
[15] Alexopoulou AN, Leao M, Caballero OL, Da Silva L, Reid L, Lakhani SR, et al. Dissecting the transcriptional networks underlying breast cancer: NR4A1 reduces the migration of normal and breast cancer cell lines. Breast Cancer Res 2010;12:R51.
[16] Yang C, Sun JJ. Mechanistic studies of cyclin-dependent kinase inhibitor 3 (CDKN3) in colorectal cancer. Asian Pac J Cancer Prev 2015;16:965–70.
[17] Li T, Xue H, Guo Y, Guo K. CDKN3 is an independent prognostic factor and promotes ovarian carcinoma cell proliferation in ovarian cancer. Oncol Rep 2014;31:1825–31.
[18] Yu D, Li J, Han Y, Liu S, Xiao N, Li Y, et al. Gene expression profiles of ERCC1, TYMS, RRM1, TUBB3 and EGFR in tumor tissue from non-small cell lung cancer patients. Chin Med J (Engl) 2014;127:1464–8.
[19] Liao W, Liu W, Yuan Q, Liu X, Ou Y, He S, et al. Silencing of DLGAP5 by siRNA significantly inhibits the proliferation and invasion of hepatocellular carcinoma cells. PLoS One 2013;8:e80789.
[20] Wang Y, Lee YM, Baitsch L, Huang A, Xiang Y, Tong H, et al. MELK is an oncogenic kinase essential for mitotic progression in basal-like breast cancer cells. Elife 2014;3:e01763.
[21] McKay SC, Unger K, Pericleous S, Stamp G, Thomas G, Hutchins RR. Array comparative genomic hybridization identifies novel potential therapeutic targets in cholangiocarcinoma. HPB (Oxford) 2011;13:309–19.
[22] Duangkumpha K, Techasen A, Loilome W, Namwat N, Thanan R, Khuntikeo N. BMP-7 blocks the effects of TGF-beta-induced EMT in cholangiocarcinoma. Tumour Biol 2014;35:9667–76.
[23] Adachi T, Eguchi S. Lymph node dissection for intrahepatic cholangiocarcinoma: a critical review of the literature to date. J Hepatobiliary Pancreat Sci 2014;21:162–8.
[24] Li Z, Biswas S, Liang B, Zou X, Shan L, Li Y, et al. Integrin beta6 serves as an immunohistochemical marker for lymph node metastasis and promotes cell invasiveness in cholangiocarcinoma. Sci Rep 2016;6:30081.
[25] Hu Y, Tang H. MicroRNAs regulate the epithelial to mesenchymal transition (EMT) in cancer progression. Microrna 2014;3:108–17.
[26] Li W, Ma J, Ma Q, Li B, Han L, Liu J, et al. Resveratrol inhibits the epithelial-mesenchymal transition of pancreatic cancer cells via suppression of the PI-3K/Akt/NF-kappaB pathway. Curr Med Chem 2013;20:4185–94.
[27] Cao M, Seike M, Soeno C, Mizutani H, Kitamura K, Minegishi Y, et al. MiR-23a regulates TGF-beta-induced epithelial-mesenchymal transition by targeting E-cadherin in lung cancer cells. Int J Oncol 2012;41:869–75.
[28] Jiang SB, He XJ, Xia YJ, Hu WJ, Luo JG, Zhang J, et al. MicroRNA-145-5p inhibits gastric cancer invasiveness through targeting N-cadherin and ZEB2 to suppress epithelial-mesenchymal transition. Onco Targets Ther 2016;9:2305–15.
[29] Yamasaki T, Seki N, Yamada Y, Yoshino H, Hidaka H, Chiyomaru T, et al. Tumor suppressive microRNA138 contributes to cell migration and invasion through its targeting of vimentin in renal cell carcinoma. Int J Oncol 2012;41:805–17.
[30] Wang Q, Tang H, Yin S, Dong C. Downregulation of microRNA-138 enhances the proliferation, migration and invasion of cholangiocarcinoma cells through the upregulation of RhoC/p-ERK/MMP-2/MMP-9. Oncol Rep 2013;29:2046–52.
[31] Wermke M, Camgoz A, Paszkowski-Rogacz M, Thieme S, von Bonin M, Dahl A, et al. RNAi profiling of primary human AML cells identifies ROCK1 as a therapeutic target and nominates fasudil as an antileukemic drug. Blood 2015;125:3760–8.
[32] Hsieh CL, Lin CL, Liu H, Chang YJ, Shih CJ, Zhong CZ, et al. WDHD1 modulates the post-transcriptional step of the centromeric silencing pathway. Nucleic Acids Res 2011;39:4048–62.
[33] Shen PF, Chen XQ, Liao YC, Chen N, Zhou Q, Wei Q, et al. MicroRNA-494-3p targets CXCR4 to suppress the proliferation, invasion, and migration of prostate cancer. Prostate 2014;74:756–67.
[34] Yang A, Wang X, Yu C, Jin Z, Wei L, Cao J, et al. microRNA-494 is a potential prognostic marker and inhibits cellular proliferation, migration and invasion by targeting SIRT1 in epithelial ovarian cancer. Oncol Lett 2017;14:3177–84.
[35] Liu Y, Li X, Zhu S, Zhang JG, Yang M, Qin Q, et al. Ectopic expression of miR-494 inhibited the proliferation, invasion and chemoresistance of pancreatic cancer by regulating SIRT1 and c-Myc. Gene Ther 2015;22:729–38.
[36] Yoshizawa-Sugata N, Masai H. Roles of human AND-1 in chromosome transactions in S phase. J Biol Chem 2009;284:20718–28.
[37] Yu M, Bardia A, Wittner BS, Stott S, Smas M, Ting D, et al. Circulating breast tumor cells exhibit dynamic changes in epithelial and mesenchymal composition. Science 2013;339:580–4.
[38] Chou CC, Lee KH, Lai IL, Wang D, Mo X, Kulp SK, et al. AMPK reverses the mesenchymal phenotype of cancer cells by targeting the Akt-MDM2-Foxo3a signaling axis. Cancer Res 2014;74:4783–95.
[39] Hu F, Guo XL, Zhang SS, Zhao QD, Li R, Xu Q, et al. Suppression of p53 potentiates chemosensitivity in nutrient-deprived cholangiocarcinoma cells via inhibition of autophagy. Oncol Lett 2017;14:1959–66.
[40] Liu Z, Jin ZY, Liu CH, Xie F, Lin XS, Huang Q, et al. MicroRNA-21 regulates biological behavior by inducing EMT in human cholangiocarcinoma. Int J Clin Exp Pathol 2015;8:4684–94.
[41] Liu N, Jiang F, He TL, Zhang JK, Zhao J, Wang C, et al. The roles of microRNA-122 overexpression in inhibiting proliferation and invasion and stimulating apoptosis of human cholangiocarcinoma cells. Sci Rep 2015;5:16566.